

# Exact scattering cross section for lattice-defect scattering of phonons using the atomistic Green's function method

Zhun-Yong Ong

*Institute of High Performance Computing (IHPC), Agency for Science,  
Technology and Research (A\*STAR), 1 Fusionopolis Way,  
#16-16 Connexis, Singapore 138632, Republic of Singapore \**

(Dated: September 17, 2024)

The use of structurally complex lattice defects, such as functional groups, embedded nanoparticles, and nanopillars, to generate phonon scattering is a popular approach in phonon engineering for thermoelectric applications. However, the theoretical treatment of this scattering phenomenon remains a formidable challenge, especially with regard to the determination of the scattering cross sections and rates associated with such lattice defects. Using the extended atomistic Green's function (AGF) method, we describe how the numerically exact mode-resolved scattering cross section  $\sigma$  can be computed for a phonon scattered by a single lattice defect. We illustrate the generality and utility of the AGF-based treatment with two examples. In the first example, we treat the isotopic scattering of phonons in a harmonic chain of atoms. In the second example, we treat the more complex problem of phonon scattering in a carbon nanotube (CNT) containing an encapsulated C60 molecule which acts as a scatterer of the CNT phonons. The application of this method can enable a more precise characterization of lattice-defect scattering and result in a more controlled use of nanostructuring and lattice defects in phonon engineering for thermoelectric applications.

## I. INTRODUCTION

The deliberate use of defects to create inhomogeneities in the crystal lattice is a known approach for reducing the lattice thermal conductivity of a semiconducting material in thermoelectrics. [1] The broken translational symmetry due to the defect results in heat-carrying phonons undergoing phonon-defect scattering, which reduces the phonon mean free path (MFP) and generates resistance to heat conduction. This reduction in the MFP in turn depends on the type and size of the defect and how phonons interact with it. In materials containing a significant concentration of defects, the reduction in the thermal conductivity can also be explained by phonon-defect scattering. [2–5]

Given the key role of phonon-defect scattering in heat conduction, [6, 7] a theoretical description of the scattering process that takes into account the atomistic structure of the defect is important. In such a description, we associate the defect with a scattering cross section  $\sigma(\nu, \mathbf{q})$  that depends on the polarization  $\nu$  and wave vector  $\mathbf{q}$  of the incident phonon. Physically, the scattering cross section  $\sigma$  corresponds to the size of the interaction of the phonon with the defect and vanishes if the phonon does not interact with the defect. It also determines the phonon-defect scattering rates that are used as inputs in semiclassical phonon transport models. [8] Therefore, the efficient computation of  $\sigma$  is important for understanding phonon-defect interactions and developing new approaches in phonon engineering for thermoelectric applications.

A popular atomistic approach to computing  $\sigma$  is the  $T$ -matrix method, [9] which depends on the changes in

the interatomic force constants and atomic masses in the lattice generated by the defect. In this method, the scattering cross section is directly computed from the diagonal matrix element of the  $T$  matrix. [10] Although this method has been applied to local site defects such as isotopes, vacancies and substitutional impurities, [11–14] it remains challenging to extend it to a more general class of structurally complex defects, such as functional groups, [15] surface nanopillars, [16–18] embedded nanoparticles, [19, 20] or molecular impurities, [21] because of the additional degrees of freedom associated with such defects.

In this paper, we propose an alternative approach for computing the scattering cross section  $\sigma$ , based on the *extended* atomistic Green's function (AGF) method, [22–24] which is commonly used to study ballistic phonon transport [22, 25–29] and has also been applied to model elastic wave scattering [30] as well as to characterize the boundary roughness scattering of phonons. [31, 32] In the extended AGF method, which is a development of the original AGF method introduced by Mingo and Yang for treating the total phonon transmission in nanowires, [25] mode-resolved quantities, such as the scattering amplitudes as well as mode-resolved transmission and reflection coefficients, can be calculated from the scattering  $S$  matrix. [24] The method for  $\sigma$  is based on a rigorous interpretation of the scattering amplitude and thus does not require any new computational technique as  $\sigma$  is derived from the diagonal element of the transmission matrix computed within the extended AGF method. [24] For the sake of simplicity, we limit the discussion of our proposed approach to quasi-one-dimensional systems, such as nanotubes or nanowires, although the approach can be easily extended to two or three-dimensional systems, which we briefly discuss in Appendix B.

Our proposed approach leverages on the existing AGF

---

\* ongy@ihpc.a-star.edu.sg

method and enables the rapid computation of scattering cross sections and rates which can be used to determine the reduction in phonon MFPs and facilitate semi-classical phonon Boltzmann transport equation (BTE) modeling of phonon transport in lattices with defects. Although defects destroy the translational symmetry of the lattice, we can treat the defects as randomly distributed, independent perturbations to the translationally symmetric defect-free lattice, of which the eigenmodes are well-defined as phonons. If we assume that the concentration of defects is dilute enough for multiple scattering and interference effects between scatterers to be neglected, [8, 9] then the corresponding total defect scattering rate  $\Gamma_{\text{defect}}$  for these phonons can be described by summing over the scattering cross section and rate of each defect. In the phonon BTE, we can model the reduction in the phonon lifetime and the lattice thermal conductivity, because the inverse lifetime for the phonon is given by  $\tau^{-1} = \Gamma_{\text{phonon}} + \Gamma_{\text{defect}}$ , where  $\Gamma_{\text{phonon}}$  is the scattering rate due to anharmonic phonon interactions. In systems with a higher concentration of defects, we cannot ignore multiple scattering and alternative phonon transport models should be used, because the effects of localization [33] may play a significant role in phonon transport. [34, 35]

Before we describe the methodology for computing  $\sigma$ , we give an intuitive explanation of how it works. In the AGF framework, the system is partitioned into the left lead, the device region containing the scatterer, and the right lead. As an incoming phonon mode propagates from one lead across the inhomogeneity within the device region and towards the other lead, part of its flux is scattered by the inhomogeneity while the remaining part of it is transmitted into the other lead. As a result of the interaction with the inhomogeneity, the transmission amplitude, which characterizes the outgoing phonon wave function, acquires an additional phase factor in its amplitude, which we can determine from the  $S$  matrix. Because the  $S$  matrix is unitary and is essentially a book-keeping device that connects the incoming amplitudes to the outgoing amplitudes [24], this phase factor allows us to determine the *change* in the phonon wave function due to scattering, from which we can find the scattering cross section  $\sigma$  using the optical theorem. Since we only examine the amplitude change in the outgoing phonon wave function in the lead, we can thus treat the device as a *black box* so long as it has the same length as its homogeneous counterpart. This treatment is more akin to the analysis of the asymptotic behavior of the scattered wave function in scattering problems. [36, 37] It is more flexible as we are less constrained by the structure of the complex defect, compared to the  $T$  matrix approach where one has to map the perturbed degrees of freedom to those of the homogeneous system and to compute directly the  $T$  matrix element associated with the perturbation.

The organization of this paper is as follows. We first describe the theoretical basis for this method of computing  $\sigma$ . We derive the key formula for the scattering

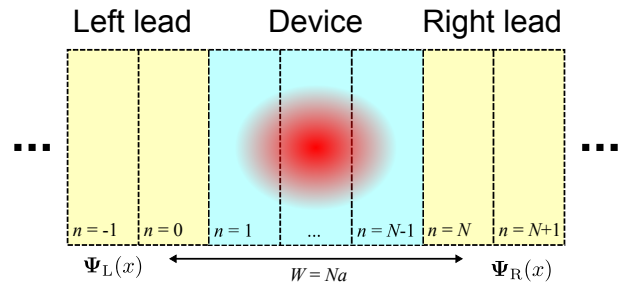


Figure 1. Schematic of layered system in the AGF method. The inhomogeneity or defect, which is represented by the red-shaded oval, is contained within the layers  $n = 1$  to  $N - 1$  which correspond to the device region. The distance between the left and right leads is  $W = Na$ .

cross section, given in Eq. (12), from the diagonal element of the transmission matrix. Next, we illustrate the utility of the method using two examples. The first example is the monoatomic harmonic chain with a single isotopic impurity while the second example consists of the (10,10) armchair carbon nanotube (CNT) with an encapsulated C60 molecule acting as the scatterer. In the second example, we compute and analyze how the scattering cross sections associated with the C60 molecule depend strongly on the polarization and atomic motion of the incident phonon modes in the CNT, especially for the low-frequency phonon subbands.

## II. THEORETICAL BASIS OF AGF-BASED APPROACH

In this section, we derive the formula for the scattering cross section by analyzing how the phonon wave function is perturbed by scattering in one dimension. Related ideas are discussed in the pedagogical review by Boya [38] although they apply only to continuous systems, such as the Schrodinger equation, and not to the discrete lattice-type system that the AGF method is designed for.

In the AGF method, [23, 24] which is outlined in Appendix A, we arrange the degrees of freedom in an infinite array of layers, which we enumerate as  $n = -\infty, \dots, 0, 1, \dots, \infty$  and assume are evenly spaced with an interlayer distance of  $a$ , as shown in Fig. 1. Thus, we can associate a discrete coordinate  $x = na$  with the center of the  $n$ -th layer. As before, we partition the system into three subsystems: the left lead ( $n \leq 0$ ), the device ( $1 < n < N - 1$ ), and the right lead ( $n \geq N$ ). In the left and right leads which are homogeneous and identical to one another, each layer acts as a unit cell, has  $l$  degrees of freedom and is identical to the other cells in the lead. In the device, the layers are not necessarily homogeneous even though they are spaced evenly and can accommodate the additional degrees of freedom associated with an inhomogeneity. In our derivation, we discuss the scattering cross section associated with the inhomogeneity for an incoming phonon propagating rightward from the left

lead towards the device.

### A. Total outgoing phonon flux from scattering

In the left lead ( $n \leq 0$ ), we associate the incident eigenwave  $\Psi_{\text{inc}}(x)$  with a phonon mode of wave vector of  $k$ , branch index  $\nu$  ( $1 \leq \nu \leq l$ ), frequency  $\omega_{\nu,k}$  and group velocity  $v_{\nu,k} > 0$ . For convenience, we use  $\nu k$  to label the phonon modes. We write the *flux-normalized* [39] phonon ‘wave function’  $\Psi_{\text{L}}(x)$  in the left lead as the sum of the incident and scattered waves:

$$\Psi_{\text{L}}(x) = \Psi_{\text{inc}}^{\text{L}}(x) + \Psi_{\text{scatt}}^{\text{L}}(x), \quad (1)$$

where  $\Psi_{\text{inc}}^{\text{L}}(x) = \Phi_{\nu k}(x) \equiv \sqrt{|v_{\nu k}|} \mathbf{u}_{\nu k}(x) e^{ikx}$  represents the incident  $\nu k$  phonon mode [40] with group velocity  $v_{\nu k}$  and  $\mathbf{u}_{\nu k}(x)$  denotes its Bloch function satisfying the relationship  $\mathbf{u}_{\nu k}(x) = \mathbf{u}_{\nu k}(x+a)$ . Because of flux normalization, Eq. (1) only contains the contribution from the propagating modes and none from the evanescent modes. In the absence of scattering, the phonon wave function at any two layers at  $x$  and  $x'$  only differ by a phase factor determined by its wave vector, i.e.,  $\Psi_{\text{L}}(x) = \Psi_{\text{L}}(x') e^{ik(x-x')}$ .

The Bloch function  $\mathbf{u}_{\nu k}(x)$  is a column vector whose  $l$  elements correspond to the displacement degrees of freedom in a unit cell. Thus, all the phonon wave functions are also column vectors. On the righthand side (RHS) of Eq. (1),  $\Psi_{\text{scatt}}^{\text{L}}(x)$  represents the *scattered* wave in the left lead and is given by

$$\Psi_{\text{scatt}}^{\text{L}}(x) = \sum_{\nu'k'} S(\nu'k', \nu k) \Phi_{\nu'k'}(x) \Theta(-v_{\nu'k'}), \quad (2)$$

which is written as a sum of the *reflected* leftward-propagating flux-normalized  $\nu'k'$  eigenmodes associated with the scattering amplitudes  $S(\nu'k', \nu k)$ . [41] The sum over  $\nu'k'$  in Eq. (2) is over all possible branches and wave vectors at the incident phonon frequency  $\omega_{\nu k}$ , i.e.,  $\omega_{\nu'k'} = \omega_{\nu k}$ . We can associate two fluxes with the left-lead wave function: one from the incident mode and the other from the modes reflected from the device into the left lead. The normalized incident flux is  $j_{\text{inc}}^{\text{L}}(\nu k) = 1$  while the reflected flux is

$$j_{\text{scatt}}^{\text{L}}(\nu k) = \sum_{\nu'k'} |S(\nu'k', \nu k)|^2 \Theta(-v_{\nu'k'}). \quad (3)$$

In the right lead ( $n \geq N$ ), we can likewise write the *flux-normalized* phonon wave function as the sum of transmitted rightward-propagating fluxes, i.e.,

$$\Psi_{\text{R}}(x) = \sum_{\nu'k'} S(\nu'k', \nu k) \Phi_{\nu'k'}(x) e^{-ik'W} \Theta(v_{\nu'k'}). \quad (4)$$

The RHS of Eq. (4) contains the incident and outgoing forward-scattered wave functions. Each summand

has a phase factor of  $e^{-ik'W}$ , where  $W$  denotes the width of the scatterer and is taken as the distance between the lead edges (from  $n = 0$  in the left lead to  $n = N$  in the right lead), so we have  $W = Na$ . In the absence of a scatterer (e.g. homogeneous waveguide), the forward-scattering amplitude in the right lead is  $\bar{S}(\nu'k', \nu k) = \delta_{\nu'\nu} \delta_{k',k} e^{ik'W}$  where  $\delta_{k',k}$  denotes the Kronecker delta function, and we recover the solution  $\bar{\Psi}_{\text{R}}(x) = \sum_{\nu'k'} \bar{S}(\nu'k', \nu k) \Phi_{\nu'k'} e^{-ik'W} \Theta(v_{\nu'k'}) = \Phi_{\nu k}(x)$ , which is just the incident eigenmode.

Like in Eq. (1), we can express Eq. (4) as the sum of the incident and scattered wave function or

$$\bar{\Psi}_{\text{R}}(x) = \bar{\Psi}_{\text{inc}}^{\text{R}}(x) + \Psi_{\text{scatt}}^{\text{R}}(x), \quad (5)$$

where  $\bar{\Psi}_{\text{inc}}^{\text{R}}(x) = \bar{\Psi}_{\text{R}}(x)$  is the incident eigenwave. This implies that the scattered wave function in the right lead is the remainder or  $\Psi_{\text{scatt}}^{\text{R}}(x) = \bar{\Psi}_{\text{R}}(x) - \bar{\Psi}_{\text{inc}}^{\text{R}}(x) = \sum_{\nu'k'} [S(\nu'k', \nu k) - \bar{S}(\nu'k', \nu k)] \Phi_{\nu'k'}(x) e^{-ik'W} \Theta(v_{\nu'k'})$ . Therefore, the associated flux for  $\Psi_{\text{scatt}}^{\text{R}}(x)$ , which represents the scattered flux exiting into the right lead, is

$$j_{\text{scatt}}^{\text{R}}(\nu k) = \sum_{\nu'k'} |S(\nu'k', \nu k) - \bar{S}(\nu'k', \nu k)|^2 \Theta(v_{\nu'k'}). \quad (6)$$

The total outgoing flux from scattering in the left and right leads is the sum of the outgoing scattered fluxes, i.e.,  $j_{\text{scatt}}(\nu k) = j_{\text{scatt}}^{\text{L}} + j_{\text{scatt}}^{\text{R}} = \sum_{\nu'k'} |S(\nu'k', \nu k) - \bar{S}(\nu'k', \nu k)|^2$ , which can be expanded to yield a sum with three terms in the summand, i.e.,

$$j_{\text{scatt}}(\nu k) = \sum_{\nu'k'} \{ |S(\nu'k', \nu k)|^2 + |\bar{S}(\nu'k', \nu k)|^2 - 2\text{Re}[S(\nu'k', \nu k) \bar{S}(\nu'k', \nu k)^*] \}.$$

The sum over each of the first two terms yields a value of unity because the unitarity of the  $S$  matrix implies that  $\sum_{\nu'k'} |S(\nu'k', \nu k)|^2 = \sum_{\nu'k'} |\bar{S}(\nu'k', \nu k)|^2 = 1$ . The sum over the remaining term yields  $-2\text{Re}[S(\nu k, \nu k) \bar{S}(\nu k, \nu k)^*]$ , given that  $\bar{S}(\nu'k', \nu k) = 0$  for  $\nu'k' \neq \nu k$ . Hence, we obtain

$$j_{\text{scatt}}(\nu k) = 2\text{Re} \left[ 1 - \frac{S(\nu k, \nu k)}{\bar{S}(\nu k, \nu k)} \right]. \quad (7)$$

The expression in Eq. (7) relates the total outgoing flux from scattering to the transmission amplitude  $S(\nu k, \nu k)$ . In the absence of any scatterer, Eq. (7) vanishes as expected since  $S(\nu k, \nu k) = \bar{S}(\nu k, \nu k)$ . Although this is not immediately obvious, Eq. (7) is just a restatement of the well-known *optical theorem* for a one-dimensional multimodal system. For convenience, we define the *forward-scattering amplitude*  $\mathcal{F}(\nu k)$  via the relationship  $S(\nu k, \nu k) = \bar{S}(\nu k, \nu k)[1 + \mathcal{F}(\nu k)]$  or

$$\mathcal{F}(\nu k) = S(\nu k, \nu k) e^{-ikW} - 1. \quad (8)$$

This allows us to simplify Eq. (7) to obtain the compact expression  $j_{\text{scatt}}(\nu k) = -2\text{Re}[\mathcal{F}(\nu k)]$ .

## B. Scattering cross section from the transmission-matrix diagonal element

Given that the incident wave function is  $\Psi_{\text{inc}}(x) = \Phi_{\nu k}(x)$ , the incoming flux for the incident  $\nu k$  mode is  $j_{\text{inc}} = 1$ . Therefore, the scattering cross section associated with the scatterer between the two leads is

$$\sigma(\nu k) = \frac{j_{\text{scatt}}}{j_{\text{inc}}} A = -2A \text{Re}[\mathcal{F}(\nu k)], \quad (9)$$

where  $A$  denotes the *geometrical cross section* of the system. It is worth remarking that the expression in Eq. (9) agrees with that obtained by Boya and Murray [37] for quantum-mechanical scattering in a continuous system, even though the derivation leading to Eq. (9)

---

To find  $S(\nu k, \nu k)$  for the  $\nu k$  mode in the left lead, we use the AGF method to compute the  $l \times l$  transmission matrix for the inhomogeneous waveguide, given by [23, 24]

$$\mathbf{t}_{\text{RL}}(\omega) = \frac{2i\omega}{a} [\mathbf{V}_{\text{R}}^{\text{ret}}(+)]^{1/2} [\mathbf{U}_{\text{R}}^{\text{ret}}(+)]^{-1} \mathbf{G}_{\text{RL}}^{\text{ret}} [\mathbf{U}_{\text{L}}^{\text{adv}}(-)]^{-1} [\mathbf{V}_{\text{L}}^{\text{adv}}(-)]^{1/2}, \quad (10)$$

where  $\omega = \omega_{\nu k}$  and  $\mathbf{G}_{\text{RL}}^{\text{ret}}$  denotes the Green's function between the rightmost left-lead ( $n = 0$ ) and the leftmost right-lead ( $n = N$ ) layers. In Eq. (10),  $\mathbf{V}_{\text{R}}^{\text{ret}}(+)$  and  $\mathbf{V}_{\text{L}}^{\text{adv}}(-)$  correspond to the velocity matrices for the outgoing right-lead phonons and the incoming left-lead phonons, respectively, while  $\mathbf{U}_{\text{R}}^{\text{ret}}(+)$  and  $\mathbf{U}_{\text{L}}^{\text{adv}}(-)$  correspond to the outgoing right-lead eigenmodes and the incoming left-lead eigenmodes, respectively. A more detailed description of these matrices is given in Eqs. (A6)-(A8) in Appendix A. The transmission matrix element  $[\mathbf{t}_{\text{RL}}(\omega)]_{pq}$  connects the flux amplitude of the  $p$ -th outgoing right-lead modes to the  $q$ -th incoming left-lead modes for  $p, q = 1, \dots, l$ . Because the left and right leads are identical, the set of incoming *extended* left-lead modes, as indexed by  $\nu k$ , is the same as the set of outgoing extended right-lead modes, and we can order the extended phonon modes by their wave vectors such that  $k_1 < k_2 < \dots$

If we discard the evanescent modes and order the row and column indices according to the size of  $k$ , then we can express Eq. (10) as a  $\bar{l} \times \bar{l}$  matrix

$$\bar{\mathbf{t}}_{\text{RL}}(\omega) = \begin{pmatrix} S(\nu_1 k_1, \nu_1 k_1) & \cdots & S(\nu_1 k_1, \nu_{\bar{l}} k_{\bar{l}}) \\ \vdots & \ddots & \vdots \\ S(\nu_{\bar{l}} k_{\bar{l}}, \nu_1 k_1) & \cdots & S(\nu_{\bar{l}} k_{\bar{l}}, \nu_{\bar{l}} k_{\bar{l}}) \end{pmatrix}, \quad (11)$$

where  $\bar{l} \leq l$  is the number of *extended propagating* incoming or outgoing phonon modes at frequency  $\omega$ . Using Eqs. (8) and (9), we obtain the scattering cross section for the incoming  $\nu_p k_p$  phonon ( $1 \leq p \leq \bar{l}$ ):

$$\sigma(\nu_p k_p) = 2A \text{Re}(1 - [\bar{\mathbf{t}}_{\text{RL}}(\omega)]_{pp} e^{-ik_p W}). \quad (12)$$

In the absence of any scattering, the expression for  $\sigma(\nu_p k_p)$  in Eq. (12) vanishes as expected, because  $[\bar{\mathbf{t}}_{\text{RL}}(\omega)]_{pp} = e^{ik_p W}$  which is equal to the phase change of the phonon wave function as it moves from layer  $n = 0$  to layer  $n = N$ .

Here, we note one limitation of our method for calculating the scattering cross section. In Eq. (10), the transmission matrix depends on the phonon group velocities. Hence, the scattering cross section is ill-defined

is purely classical. This suggests that the generalized optical theorem obtained in Ref. [37] can be extended to non-quantum-mechanical settings.

In the absence of a scatterer, Eq. (9) yields  $\sigma = 0$  as expected since  $S(\nu k, \nu k) = \bar{S}(\nu k, \nu k)$  and  $\mathcal{F}(\nu k) = 0$ . On the other hand, we note that  $\sigma \leq 4A$ , i.e., the maximum value of the total scattering cross section can be as large as *four times* the geometrical cross section when  $S(\nu k, \nu k) = -\bar{S}(\nu k, \nu k)$  and  $\mathcal{F}(\nu k) = -2$ . [38] While it appears to be counterintuitive and even possibly unphysical, this result also occurs in quantum mechanics for scattering by a hard sphere in three dimensions. [42] This is a consequence of our partitioning of the wave function in  $\Psi_{\text{L}}(x)$  and  $\Psi_{\text{R}}(x)$  into two *non-orthogonal* components: the incident wave  $\Psi_{\text{inc}}$  and the scattered wave  $\Psi_{\text{scatt}}$  which represents the part of the original wave that has been perturbed.

---

for eigenmodes that have zero group velocity and cannot propagate spatially.

## III. EXAMPLES

### A. Monoatomic harmonic chain with a single isotopic impurity

To illustrate the AGF method for calculating the scattering cross section, we apply it to the simple archetypal example [43] of phonon scattering by a single isotopic impurity of mass  $m_{\text{C}}$  in a monoatomic harmonic chain with an interatomic distance of  $a$ , as shown in Fig. 2(a). In this system, we treat the isotopic impurity as the device; the mass and interatomic force constants of the rest of the system are given by  $m$  and  $\zeta$ , respectively. For the monoatomic harmonic chain, the phonon dispersion is given by  $\omega(k)^2 = \omega_m^2 \sin^2(ka/2)$ , where  $\omega_m = 2\sqrt{\zeta/m}$ , and the phonon group velocity is given by  $v(\omega) = \pm \frac{1}{2} a (\omega_m^2 - \omega^2)^{1/2}$ . As there is only one phonon branch, all the terms in Eq. (10) are scalars. Thus,

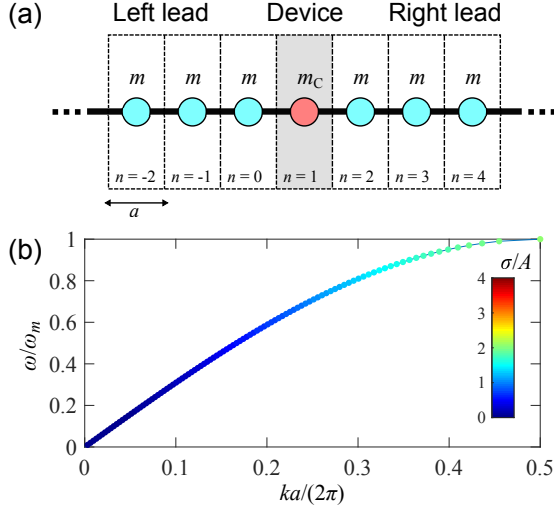


Figure 2. (a) Schematic of monoatomic harmonic chain with a single isotopic impurity  $m_c$ . (b) Plot of the  $\omega - k$  phonon dispersion for the single phonon branch and the normalized scattering cross section  $\sigma/A$  values of the phonon eigenmodes, with values indicated by the color bar, for  $\epsilon = 1$ .

Eq. (10) simplifies to  $t_{\text{RL}}(\omega) = i\omega(\omega_m^2 - \omega^2)^{1/2}G_{\text{RL}}^{\text{ret}}(\omega)$ .

### 1. Analytical expression for Green's function

At frequency  $\omega < \omega_m$ , the Green's function of the device is given by [28]

$$G_C^{\text{ret}}(\omega) = [\omega^2 + i0^+ - \frac{2\zeta}{m_C} - \Sigma_L^{\text{ret}}(\omega) - \Sigma_R^{\text{ret}}(\omega)]^{-1},$$

where  $\Sigma_{\text{L/R}}^{\text{ret}}(\omega) = \frac{\zeta^2}{mm_C}g(\omega)$  denotes the self-energy term associated with the left/right lead and  $g(\omega) = \frac{1}{2}(\omega^2 + i0^+ - \frac{2\zeta}{m}) - \frac{1}{2}[(\omega^2 + i0^+ - \frac{2\zeta}{m})^2 - 4(\frac{\zeta}{m})^2]^{1/2}$ . The analytical expression for the Green's function  $G_{\text{RL}}^{\text{ret}}(\omega)$ , which describes the correlation between the ends of the left and right leads, is given by  $G_{\text{RL}}^{\text{ret}}(\omega) = g(\omega)H_{\text{RC}}G_C^{\text{ret}}(\omega)H_{\text{CL}}g(\omega)$ , [22–24] where  $H_{\text{RC}} = H_{\text{CL}} = \zeta/\sqrt{mm_C}$  denotes the lead-device coupling term.

### 2. Scattering cross section and rate

After some algebra, we obtain from Eq. (12) the expression for the scattering cross section of the single isotopic impurity, normalized by the geometrical cross section  $A$ ,

$$\frac{\sigma(\omega)}{A} = \frac{2\epsilon^2\omega^4}{\epsilon^2\omega^4 + \omega^2(\omega_m^2 - \omega^2)}, \quad (13)$$

where  $\epsilon = (m_C - m)^2/m^2$  is the dimensionless parameter for the mass difference. In Eq. (13),  $\sigma/A$ , which increases monotonically with  $\omega$  and is shown in Fig. 2(b) for  $\epsilon = 1$ ,

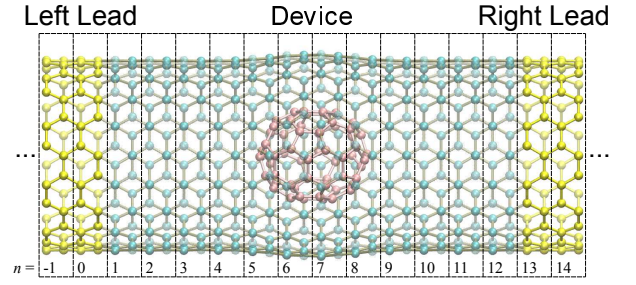


Figure 3. Schematic of the layer arrangement in the (10,10) armchair carbon nanotube with a C60 molecule (pink-shaded atoms) encapsulated within the device region (turquoise-shaded atoms) in layers  $n = 1$  to 12. The layers in the leads, which extend semi-infinitely to the left or right, are represented by the yellow-shaded atoms.

has a value between 0 (no scattering) and 2 (total scattering) and never reaches the theoretical upper bound of 4 from Eq. (9). The scattering rate is

$$\Gamma(\omega) = \frac{N_i\sigma_{\text{tot}}(\omega)v(\omega)}{NaA} = n_i \frac{\epsilon\omega^4(\omega_m^2 - \omega^2)^{1/2}}{\epsilon\omega^4 + \omega^2(\omega_m^2 - \omega^2)}, \quad (14)$$

where  $n_i = \frac{N_i}{Na}$  denotes the lineal concentration of isotopic impurities. In the  $\epsilon \ll 1$  limit, Eq. (14) reduces to

$$\Gamma(\omega) = \frac{n_i\epsilon\omega^2}{(\omega_m^2 - \omega^2)^{1/2}} + O(\epsilon^2),$$

in agreement with the result [44] obtained in Ref. [43].

## B. Carbon nanotube with an encapsulated C60 molecule

Next, we apply the AGF method to the more complex problem of a single C60 molecule encapsulated in the center of a (10,10) armchair CNT, as shown in Fig. 3. The purpose of our discussion, which is not meant to be comprehensive, is to illustrate how the scattering cross section depends on the properties of the phonon mode and its interaction with the *external* scatterer. Unlike the monoatomic chain in which the atoms can only move along the longitudinal axis and there is only one phonon branch, the CNT has 120 phonon branches because of the 40 carbon atoms in the unit cell and the three degrees of freedom in atomic motion. These differences in the atomic motion of the phonons affect their interaction with the C60 molecule. In the system shown in Fig. 3, the finite CNT region encapsulating the C60 molecule acts as the device while each lead comprises a semi-infinite homogeneous CNT, in which each layer corresponds to the unit cell. Because the C60-CNT interaction breaks the translational symmetry of the interatomic forces in the CNT, the incoming phonons from the leads are scattered

and we can associate a scattering cross section for each phonon mode of the CNT.

We model the covalent C-C bonds within the CNT or C60 molecule using the Tersoff potential optimized for graphene [45] and the weak van der Waals forces between the CNT and the C60 molecule using the Lennard-Jones (LJ) potential with parameters from Ref. [46]. In Fig. 3, the device region spans 12 layers ( $n = 1$  to 12) in the CNT as the C60 molecule couples to the atoms in them through the LJ potential. We also observe a small bulge in the CNT in the device region from the C60-CNT interaction. We optimize the structure using GULP [47] and extract the interatomic force constants needed as inputs for the AGF computations, which are described in Refs. [23, 24], and the phonon dispersion of the CNT shown in Fig. 4(a).

### 1. Distribution of mode-dependent scattering cross sections

We compute the area-normalized scattering cross section  $\sigma(\nu k)/A$  for each rightward-propagating  $\nu k$  phonon mode in the (10,10) armchair CNT using Eqs. (10) and (12) for a range of angular frequencies  $\omega$  in intervals of  $\Delta\omega = 2 \times 10^{12}$  rad/s from  $\omega = 2 \times 10^{12}$  to  $3.16 \times 10^{14}$  rad/s. At each  $\omega$ , we obtain a set of phonon modes with the wave vectors  $k_1, k_2, \dots$ , which we plot as solid circles in Fig. 4. As in Fig. 2, we indicate the value of  $\sigma/A$  of each mode by the color of its solid circle symbol. For ease of interpretation, the solid circle symbols are superimposed on the  $\omega - k$  phonon dispersion curves for the (10,10) armchair CNT. [48]

In Fig. 4(a), there are 66 distinct ones due to the degeneracies in the (10,10) armchair CNT. [48] At  $k = 0$  in the  $\omega \rightarrow 0$  limit, there are four acoustic phonon branches corresponding to the longitudinal acoustic (LA), the azimuthal twisting (TW) and the doubly degenerate radial transverse acoustic (TA) phonons. [49, 50] In addition, there is a breathing mode (BR) associated with the radial oscillation of the CNT at  $k = 0$ . The remaining phonon branches consist of subbands with  $\omega > 0$  at  $k = 0$ . We observe two distinct  $\sigma/A$  trends for the lower-frequency phonon subbands in Fig. 4(a). In the subbands with higher group velocities and near-linear dispersion,  $\sigma/A$  is vanishingly small because the atomic motion for the phonon modes is primarily along the longitudinal direction [48]. On the other hand, in the subbands with smaller group velocities and a more parabolic dispersion,  $\sigma/A$  increases significantly with  $\omega$ , indicating stronger interaction with the C60 molecule. For the subbands correspond to the high-frequency optical phonons, we have  $\sigma/A \sim 2$ , which indicates strong scattering.

### 2. Low-frequency phonon subbands

For a more detailed analysis of how the C60 molecule scatters different phonon modes, the low-frequency  $\sigma/A$  distribution is shown in Fig. 4(b). The individual phonon

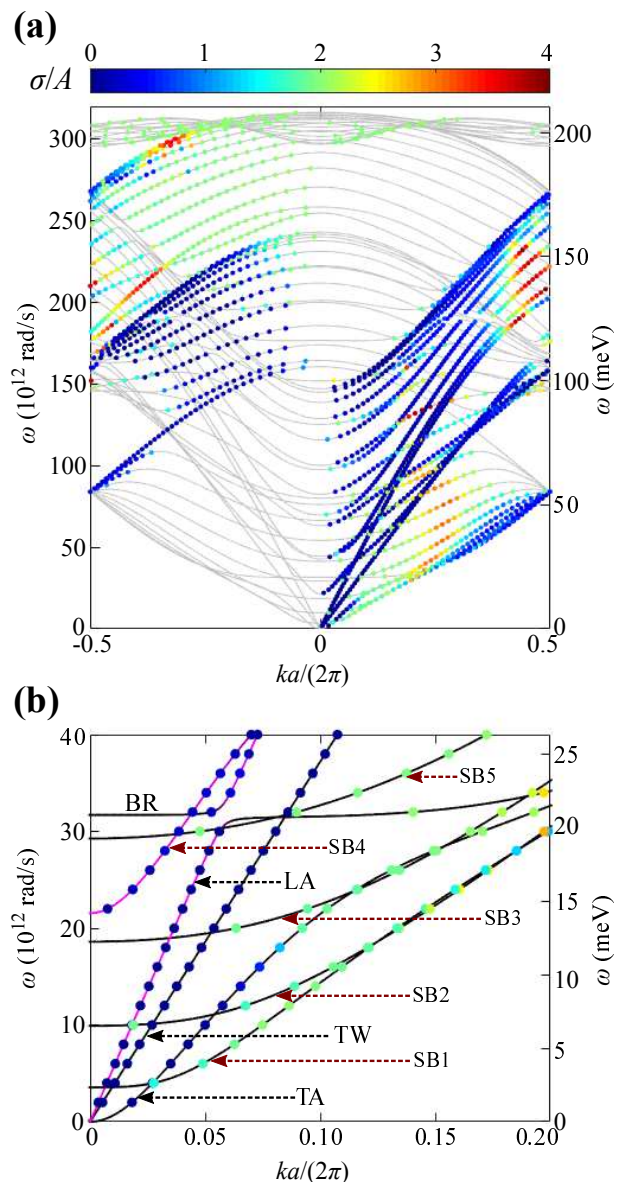


Figure 4. (a) Plot of scattering cross section  $\sigma/A$  for each rightward-propagating phonon mode (solid circle) in the (10,10) armchair CNT, distributed over the 66 distinct phonon branches. The values of  $\sigma/A$  are between 0 and 4 and are indicated by color according to the color bar. (b) The corresponding plot at low frequencies ( $\omega < 4 \times 10^{13}$  rad/s). We observe the three distinct acoustic phonon branches (LA, TW and TA) and the radial breathing mode (BR) as well as the five lowest phonon subbands which are indicated by brown dashed arrows and labeled SB1 to SB5. The phonon branches are also colored according to the percentage of their eigenmode atomic displacements parallel to the longitudinal axis, with the color varying continuously between bright magenta (100%) and black (0%).

dispersion curves for the acoustic phonons (LA, TW and TA) and the five lowest phonon subbands (SB1 to SB5) are also displayed, with the color of the individual curves indicating the percentage of the eigenmode atomic displacements parallel to the longitudinal axis. We observe that the  $\sigma/A$  values for the acoustic phonons approaches 0 in the long wavelength ( $k = 0$ ) limit and increases monotonically with  $k$ , similar to the results for the monoatomic chain in Fig. 2. In particular, the LA and TW phonons, whose atomic motions are in the longitudinal and azimuthal directions, respectively, have very small  $\sigma/A$  values which we can attribute to their weak coupling to the C60 molecule. The TA phonons however see a significant increase in  $\sigma/A$  as  $k$  increases because of the radial motion of their modes.

On the other hand, the modes in the low-frequency phonon subbands (SB1, SB2, SB3 and SB5) have a finite  $\sigma/A$  in the  $k = 0$  limit and increases with  $\omega$ . This implies that that these modes, which are polarized in the plane normal to the longitudinal axis and whose atomic motions are mainly in the radial and azimuthal directions, [46, 49, 50] are sensitive to interaction with the C60 molecule. However, in the SB4 subband, the low  $\sigma/A$  values indicate that its phonon modes, which are longitudinally polarized like those in the LA branch, interact weakly with the C60 molecule. This observation is consistent with the results for carbon nanotube peapods in Ref. [46] where the authors report a weak reduction in the low-frequency LA phonon lifetimes. The results in Fig. 4(b) support the finding that the phonon scattering by the C60 molecule is strongly dependent on phonon polarization, with phonon modes whose atomic motions have a radial component being more strongly scattered by the C60 molecule.

#### IV. SUMMARY AND CONCLUSIONS

In summary, we have shown rigorously how the mode-dependent scattering cross sections and rates in a lattice can be determined using the extended AGF method. [23, 24] This AGF-based approach allows us to treat scattering problems in which additional degrees of freedom from an external scatterer are present. Its utility is demonstrated with two examples: (1) the monoatomic harmonic chain with a single isotopic impurity, and (2) the (10,10) CNT with an encapsulated C60 molecule. In the first example, we derive the exact analytical expressions for the scattering cross section and rate. To first order in perturbation, the latter is identical to the result in Ref. [43]. In the second example, we illustrate how the scattering cross section varies with the properties of the phonon mode (phonon branch and frequency), and show how phonon modes with radial atomic motion are more strongly scattered by the C60 molecule.

This approach allows us to compute the phonon-defect scattering rates which can be used as inputs in semiclassical phonon transport models. It can also be used to study

how the atomic structure of a defect affects the scattering cross section of different phonon modes and thus enable the more controlled use of nanostructuring and lattice defects in phonon engineering for thermoelectric applications. [1] With some straightforward modification, this approach can also be extended to tightbinding lattice models to determine the scattering cross sections associated with perturbations by external degrees of freedom, because of the close analogy [26, 29, 51] between the AGF method and commonly used quantum transport models for electrons. [52, 53]

#### ACKNOWLEDGMENTS

The author acknowledges funding support from the Agency for Science, Technology and Research (A\*STAR) of Singapore with the Manufacturing, Trade and Connectivity (MTC) Programmatic Grant ‘‘Advanced Modeling Models for Additive Manufacturing’’ (Grant No. M22L2b0111) and from the Polymer Matrix Composites Program (SERC Grant No. A19C9a004).

#### Appendix A: The extended Atomistic Green’s Function method

For the convenience of the reader and the sake of completeness, we give a brief description of the extended AGF method, in which the transmission and reflection matrices can be calculated, largely following our earlier papers on extending the AGF method [23, 24]. Here, we discuss only the transmission matrices, which are relevant to Eq. (10).

In the AGF setup in Fig. 1, the system is partitioned into three subsystems: (1) the left lead, (2) the device region, and (3) the right lead. Each lead consists of a semi-infinite one-dimensional array of principal layers while the device region corresponds to layers  $n = 1$  to  $N - 1$ . In Fig. 1, the left and right leads are materially identical with the same interlayer spacing  $a_L = a_R$  and interatomic forces.

We can write the mass-normalized force-constant matrix  $\mathbf{H}$ , which represents the harmonic coupling of the entire system in Fig. 1 and has the block-tridiagonal structure, as

$$\mathbf{H} = \begin{pmatrix} \ddots & \ddots & & & & & & \\ & \ddots & \mathbf{H}_L^{00} & \mathbf{H}_L^{01} & & & & \\ & & \mathbf{H}_L^{10} & \mathbf{H}_L^{00} & \mathbf{H}_{LC} & & & \\ & & & \mathbf{H}_L^{00} & \mathbf{H}_C & \mathbf{H}_{CR} & & \\ & & & & \mathbf{H}_{RC} & \mathbf{H}_R^{00} & \mathbf{H}_R^{01} & \\ & & & & & \mathbf{H}_R^{10} & \mathbf{H}_R^{00} & \ddots \\ & & & & & & & \ddots & \ddots \end{pmatrix}, \quad (\text{A1})$$

where  $\mathbf{H}_C$ , and  $\mathbf{H}_{CL}$  ( $\mathbf{H}_{CR}$ ) are respectively the mass-normalized force-constant submatrices corresponding to the device region, and the coupling between the device region and the semi-infinite left (right) lead. We can associate each layer in Fig. 1 with a block row in  $\mathbf{H}$ . The block row submatrices  $\mathbf{H}_\alpha^{00}$  and  $\mathbf{H}_\alpha^{01}$ , where  $\alpha = L$  and  $\alpha = R$  for the left and right lead, respectively, describe the lead phonons. If we set the layers to be large enough so that only adjacent layers can couple, then  $\mathbf{H}_\alpha^{00}$  denotes to the intralayer force-constant matrix for each layer while  $\mathbf{H}_\alpha^{01}$  ( $\mathbf{H}_\alpha^{10}$ ) denotes the interlayer harmonic coupling between each layer and the layer to its right (left) in the lead. Here,  $\alpha$  is used as the dummy variable for distinguishing the leads, with  $\alpha = L$  and  $\alpha = R$  corresponding to the left and right leads, respectively. We also maintain the conceptual distinction between the left-lead and right-lead force-constant matrices of  $\mathbf{H}_\alpha^{00}$  and  $\mathbf{H}_\alpha^{01}$  even though  $\mathbf{H}_L^{00} = \mathbf{H}_R^{00}$  and  $\mathbf{H}_L^{01} = \mathbf{H}_R^{01}$  in our method for computing the scattering cross section.

We note here that in spite of the infinite number of layers making up the system, only a finite set of unique force-constant matrices ( $\mathbf{H}_C$ ,  $\mathbf{H}_{CL}$ ,  $\mathbf{H}_{CR}$ ,  $\mathbf{H}_L^{00}$ ,  $\mathbf{H}_L^{01}$ ,  $\mathbf{H}_R^{00}$  and  $\mathbf{H}_R^{01}$ ) are needed as inputs for the AGF calculation because the leads are made up of identical layers and the Hermiticity of  $\mathbf{H}$  implies that  $\mathbf{H}_{LC} = (\mathbf{H}_{CL})^\dagger$  and  $\mathbf{H}_{RC} = (\mathbf{H}_{CR})^\dagger$ , and  $\mathbf{H}_\alpha^{01} = (\mathbf{H}_\alpha^{10})^\dagger$ . For the sake of convenience, we also represent the  $N - 1$  layers in the device region by a single matrix  $\mathbf{H}_C$ .

In principle, the system dynamics are determined by the infinitely large  $\mathbf{H}$  in Eq. (A1). However, for the *effective* dynamics at a fixed frequency  $\omega$ , the lattice dynamics problem becomes more tractable as we need only to project the dynamics onto a finite portion of the system, [29, 54] corresponding to layers  $n = 0$  to  $N$  in Fig. 1, to determine phonon scattering by the device region. Hence, we can use the submatrices in Eq. (A1) to construct the *effective* harmonic matrix for this subsystem, [29]

$$\mathbf{H}' = \begin{pmatrix} \mathbf{H}'_L & \mathbf{H}'_{LC} & 0 \\ \mathbf{H}'_{CL} & \mathbf{H}'_C & \mathbf{H}'_{CR} \\ 0 & \mathbf{H}'_{RC} & \mathbf{H}'_R \end{pmatrix}, \quad (\text{A2})$$

where  $\mathbf{H}'_L = \mathbf{H}_L^{00} + \mathbf{H}_L^{10} \mathbf{g}_{L,-}^{\text{ret}} \mathbf{H}_L^{01}$  and  $\mathbf{H}'_R = \mathbf{H}_R^{00} + \mathbf{H}_R^{01} \mathbf{g}_{R,+}^{\text{ret}} \mathbf{H}_R^{10}$  correspond to the left and right edges, respectively while  $\mathbf{H}'_C = \mathbf{H}_C$  and  $\mathbf{H}'_{CL/CR} = \mathbf{H}_{CL/CR} = (\mathbf{H}'_{LC/RC})^\dagger$ . The retarded surface Green's functions  $\mathbf{g}_{L,-}^{\text{ret}}(\omega)$  and  $\mathbf{g}_{R,+}^{\text{ret}}(\omega)$  are given by

$$\mathbf{g}_{\alpha,-}^{\text{ret}} = [(\omega^2 + i0^+) \mathbf{I}_\alpha - \mathbf{H}_\alpha^{00} - \mathbf{H}_\alpha^{10} \mathbf{g}_{\alpha,-}^{\text{ret}} \mathbf{H}_\alpha^{01}]^{-1}, \quad (\text{A3a})$$

$$\mathbf{g}_{\alpha,+}^{\text{ret}} = [(\omega^2 + i0^+) \mathbf{I}_\alpha - \mathbf{H}_\alpha^{00} - \mathbf{H}_\alpha^{01} \mathbf{g}_{\alpha,+}^{\text{ret}} \mathbf{H}_\alpha^{10}]^{-1}. \quad (\text{A3b})$$

Physically, Eq. (A3a) denotes the retarded surface Green's function for a decoupled semi-infinite lattice extending infinitely to the left (denoted by the “-” in the

subscript of  $\mathbf{g}_{\alpha,-}^{\text{ret}}$ ) while Eq. (A3b) denotes the corresponding surface Green's function for a decoupled semi-infinite lattice extending infinitely to the right (denoted by the “+” in the subscript of  $\mathbf{g}_{\alpha,+}^{\text{ret}}$ ). In addition, the advanced surface Green's functions can be obtained from the Hermitian conjugates of Eq. (A3), i.e.,  $\mathbf{g}_{\alpha,-}^{\text{adv}} = (\mathbf{g}_{\alpha,-}^{\text{ret}})^\dagger$  and  $\mathbf{g}_{\alpha,+}^{\text{adv}} = (\mathbf{g}_{\alpha,+}^{\text{ret}})^\dagger$ .

Given Eqs. (A2) and (A3), we can assemble the pieces needed for the phonon scattering calculations. The first piece is the corresponding Green's function for Eq. (A2)  $\mathbf{G}^{\text{ret}} = [(\omega^2 + i0^+) \mathbf{I}' - \mathbf{H}']^{-1}$ , where  $\mathbf{I}'$  is an identity matrix of the same size as  $\mathbf{H}'$ ; the  $\mathbf{G}^{\text{ret}}$  matrix can be partitioned into blocks in the same manner as  $\mathbf{H}'$ , i.e.,

$$\mathbf{G}^{\text{ret}} = \begin{pmatrix} \mathbf{G}_L^{\text{ret}} & \mathbf{G}_{LC}^{\text{ret}} & \mathbf{G}_{LR}^{\text{ret}} \\ \mathbf{G}_{CL}^{\text{ret}} & \mathbf{G}_C^{\text{ret}} & \mathbf{G}_{CR}^{\text{ret}} \\ \mathbf{G}_{RL}^{\text{ret}} & \mathbf{G}_{RC}^{\text{ret}} & \mathbf{G}_R^{\text{ret}} \end{pmatrix}. \quad (\text{A4})$$

The next step is the computation of the advanced and retarded Bloch matrices [22, 53, 55] of the left and right leads,  $\mathbf{F}_\alpha^{\text{adv/ret}}(+)$  and  $\mathbf{F}_\alpha^{\text{adv/ret}}(-)$ , which describe the bulk translational symmetry of the layers along the direction of the heat flux and can be computed directly from the formulas:

$$\mathbf{F}_\alpha^{\text{adv/ret}}(+) = \mathbf{g}_{\alpha,+}^{\text{adv/ret}} \mathbf{H}_\alpha^{10}, \quad (\text{A5a})$$

$$\mathbf{F}_\alpha^{\text{adv/ret}}(-)^{-1} = \mathbf{g}_{\alpha,-}^{\text{adv/ret}} \mathbf{H}_\alpha^{01}. \quad (\text{A5b})$$

The bulk eigenmodes for the lead, which describe the mode-dependent atomic displacement in each layer at frequency  $\omega$ , can be determined directly from the Bloch matrices,

$$\mathbf{F}_\alpha^{\text{adv/ret}}(+) \mathbf{U}_\alpha^{\text{adv/ret}}(+) = \mathbf{U}_\alpha^{\text{adv/ret}}(+) \mathbf{\Lambda}_\alpha^{\text{adv/ret}}(+), \quad (\text{A6a})$$

$$\mathbf{F}_\alpha^{\text{adv/ret}}(-)^{-1} \mathbf{U}_\alpha^{\text{adv/ret}}(-) = \mathbf{U}_\alpha^{\text{adv/ret}}(-) \mathbf{\Lambda}_\alpha^{\text{adv/ret}}(-)^{-1}, \quad (\text{A6b})$$

where  $\mathbf{U}_\alpha^{\text{ret}}(+)$  [ $\mathbf{U}_\alpha^{\text{ret}}(-)$ ] is a matrix with its column vectors corresponding to the rightward-going (leftward-going) extended or rightward (leftward) decaying evanescent modes and has the form  $\mathbf{U}_\alpha^{\text{ret}} = (\mathbf{e}_1 \mathbf{e}_2 \dots \mathbf{e}_N)$  where  $\mathbf{e}_n$  is a normalized eigenvector of the Bloch matrix in the  $n$ -th column of  $\mathbf{U}_\alpha^{\text{ret}}(+)$  [ $\mathbf{U}_\alpha^{\text{ret}}(-)$ ]. Similarly,  $\mathbf{U}_\alpha^{\text{adv}}(-)$  [ $\mathbf{U}_\alpha^{\text{adv}}(+)$ ] is a matrix with its column vectors corresponding to rightward-going (leftward-going) extended or leftward (rightward) decaying evanescent modes. The matrix  $\mathbf{\Lambda}_\alpha^{\text{adv/ret}}(+)$  [ $\mathbf{\Lambda}_\alpha^{\text{adv/ret}}(-)$ ] is a diagonal matrix with matrix elements of the form  $e^{ik_n a}$  where  $k_n$  is the phonon wave vector corresponding to the  $n$ -th column eigenvector in  $\mathbf{U}_\alpha^{\text{adv/ret}}(+)$  [ $\mathbf{U}_\alpha^{\text{adv/ret}}(-)$ ]. In a complex pseudo-1D system such as the carbon nanotube, we can also attach to each eigenmode an extra label corresponding to the branch index  $\nu$  so that each eigenmode has a label  $\nu_n k_n$ .

The final piece of ingredient needed for the phonon scattering calculations is the diagonal velocity matrix [29,



53]

$$\mathbf{V}_\alpha^{\text{adv}/\text{ret}}(+)=\frac{ia_\alpha}{2\omega}[\mathbf{U}_\alpha^{\text{adv}/\text{ret}}(+)]^\dagger\mathbf{H}_\alpha^{01}[\mathbf{g}_{\alpha,+}^{\text{adv}/\text{ret}}-\mathbf{g}_{\alpha,+}^{\text{ret}/\text{adv}}]^\dagger\mathbf{H}_\alpha^{10}\mathbf{U}_\alpha^{\text{adv}/\text{ret}}(+), \quad (\text{A7})$$

which has group velocities of the eigenvectors in  $\mathbf{U}_\alpha^{\text{adv}/\text{ret}}(+)$  as its diagonal elements. Likewise,  $\mathbf{V}_\alpha^{\text{adv}/\text{ret}}(-)$  is defined as

$$\mathbf{V}_\alpha^{\text{adv}/\text{ret}}(-)=-\frac{ia_\alpha}{2\omega}[\mathbf{U}_\alpha^{\text{adv}/\text{ret}}(-)]^\dagger\mathbf{H}_\alpha^{10}[\mathbf{g}_{\alpha,-}^{\text{adv}/\text{ret}}-\mathbf{g}_{\alpha,-}^{\text{ret}/\text{adv}}]^\dagger\mathbf{H}_\alpha^{01}\mathbf{U}_\alpha^{\text{adv}/\text{ret}}(-). \quad (\text{A8})$$

For evanescent modes, the group velocity is always zero while for propagating modes that contribute to the heat flux, the group velocity is positive (negative) in  $\mathbf{V}_\alpha^{\text{ret}}(+)$  and  $\mathbf{V}_\alpha^{\text{adv}}(-)$  [ $\mathbf{V}_\alpha^{\text{ret}}(-)$  and  $\mathbf{V}_\alpha^{\text{adv}}(+)$ ]. In addition, we define the diagonal matrices  $\tilde{\mathbf{V}}_\alpha^{\text{adv}/\text{ret}}(+)$  and  $\tilde{\mathbf{V}}_\alpha^{\text{adv}/\text{ret}}(-)$  in which their nonzero diagonal matrix elements are the inverse of those of  $\mathbf{V}_\alpha^{\text{adv}/\text{ret}}(+)$  and  $\mathbf{V}_\alpha^{\text{adv}/\text{ret}}(-)$ , respectively.

From Eqs. (A3) to (A8), we construct the flux-normalized transmission matrix used in Eq. (10):

$$\mathbf{t}_{\text{RL}}=\frac{2i\omega}{\sqrt{a_{\text{R}}a_{\text{L}}}}[\mathbf{V}_{\text{R}}^{\text{ret}}(+)]^{1/2}[\mathbf{U}_{\text{R}}^{\text{ret}}(+)]^{-1}\times\mathbf{G}_{\text{RL}}^{\text{ret}}[\mathbf{U}_{\text{L}}^{\text{adv}}(-)]^{-1}[\mathbf{V}_{\text{L}}^{\text{adv}}(-)]^{1/2}. \quad (\text{A9})$$

Each row of  $\mathbf{t}_{\text{RL}}$  corresponds to either a transmitted right-lead extended or evanescent mode. For an outgoing evanescent mode, the row elements and group velocity, given by the diagonal element of  $\mathbf{V}_{\text{R}}^{\text{ret}}(+)$ , are zero. Conversely, each column of  $\mathbf{t}_{\text{RL}}$  corresponds to either an incoming left-lead extended or evanescent mode, and the column elements and group velocity of the evanescent modes, given by the diagonal element of  $\mathbf{V}_{\text{L}}^{\text{adv}}(-)$ , are zero. If the  $m$ -th row and  $n$ -th column of  $\mathbf{t}_{\text{RL}}$  correspond to extended transmitted and incoming modes, then  $|\mathbf{t}_{\text{RL}}|_{mn}|^2$  gives us the probability that the incoming left-lead phonon is transmitted across the device region into the right-lead phonon. Similarly, we can define the flux-normalized transmission matrix for phonon transmission from the right to the left lead:

$$\mathbf{t}_{\text{LR}}=\frac{2i\omega}{\sqrt{a_{\text{L}}a_{\text{R}}}}[\mathbf{V}_{\text{L}}^{\text{ret}}(-)]^{1/2}[\mathbf{U}_{\text{L}}^{\text{ret}}(-)]^{-1}\times\mathbf{G}_{\text{LR}}^{\text{ret}}[\mathbf{U}_{\text{R}}^{\text{adv}}(+)]^{-1}[\mathbf{V}_{\text{R}}^{\text{adv}}(+)]^{1/2}. \quad (\text{A10})$$

## Appendix B: Generalization to two or three dimensions

Although the examples given in this paper are only applied to 1D (monotomic chain) or pseudo-1D systems

(e.g. carbon nanotube), the generalization of our method to 2D or 3D systems merits a more detailed discussion. It should be noted that the original AGF method [28] has been applied to the investigation of phonon transport in 2D and 3D systems [27, 56, 57] and its extension, as described in Appendix A, can be applied in a straightforward manner. The key difference between a 1D system and its 2D or 3D counterpart is that in the latter, each phonon eigenmode of the lead, from Eq. (A6), is characterized by its transverse momentum ( $k_y, k_z$ ) in addition to its longitudinal momentum  $k_x$ , frequency  $\omega$  and branch index  $\nu$ . Examples of the characterization of lead phonon eigenmodes by their transverse momenta can be found in Refs. [24, 31, 32, 58].

For simplicity, we will only sketch the 2D case as the 3D case can be generalized from the 2D case. In a 2D system such as a graphene sheet with a finite but sufficiently large geometrical width of  $\mathcal{T}$  and coplanar with the  $x-y$  plane, we impose periodic boundary conditions in the transverse ( $y$ ) direction and open boundary conditions in the longitudinal ( $x$ ) direction. We should more accurately characterize the system as being *quasi*-2D because of its finite width. When  $\mathcal{T}$  is sufficiently large, the computed scattering of cross section is expected to approach the exact value.

In the case of a single-layer graphene, the leads are pristine graphene sheets semi-infinite in the longitudinal direction while the device is a graphene sheet of finite length with either a defect or has some external scatterer (e.g. a functional group) attached to it. Hence, in such a system, every extended phonon mode of the lead is a 2D phonon mode and is characterized by a discrete transverse momentum  $k_y$ , [57] which is given by  $2\pi n/\mathcal{T}$  for  $n=0, \pm 1, \pm 2, \dots$ , in addition to its longitudinal momentum  $k_x$ , which is a function of  $\omega$  and  $k_y$ . In a phonon branch with the linear dispersion  $\omega=ck$  where  $c$  is the group velocity, the longitudinal momenta  $k_x$  of the eigenmodes at frequency  $\omega$  would be discretized and given by  $k_x=\pm\sqrt{(\omega/c)^2-(2\pi n/\mathcal{T})^2}$  for  $n=0, \pm 1, \dots, \pm N$  and  $N=\lfloor\frac{\omega\mathcal{T}}{2\pi c}\rfloor$ . In the  $\mathcal{T}\rightarrow\infty$  limit, we recover the idealized 2D system and the transverse and longitudinal momenta are continuous.

After labeling each lead phonon eigenmode by its transverse momentum, we can compute its scattering cross section using Eq. (12) with the geometrical cross section  $A$  replaced by  $\mathcal{T}$ . In the case of a 2D system, we can rewrite Eq. (11) as:

$$\bar{\mathbf{t}}_{\text{RL}}(\omega)=\begin{pmatrix} S(\nu_1\mathbf{k}_1, \nu_1\mathbf{k}_1) & \cdots & S(\nu_1\mathbf{k}_1, \nu_l\mathbf{k}_l) \\ \vdots & \ddots & \vdots \\ S(\nu_l\mathbf{k}_l, \nu_1\mathbf{k}_1) & \cdots & S(\nu_l\mathbf{k}_l, \nu_l\mathbf{k}_l) \end{pmatrix}, \quad (\text{B1})$$

where the momentum of the phonon mode is represented by a vector  $\mathbf{k}=(k_x, k_y)$  instead of a scalar  $k$ , with  $\mathbf{k}=\mathbf{k}_n$  and  $1\leq n\leq\bar{l}$ . From Eq. (B1), we can determine the scattering cross sections  $\sigma(\nu_1\mathbf{k}_1)$  to  $\sigma(\nu_l\mathbf{k}_l)$ .

- 
- [1] Zihang Liu, Jun Mao, Te Huan Liu, Gang Chen, and Zhifeng Ren, “Nano-microstructural control of phonon engineering for thermoelectric energy harvesting,” *MRS Bulletin* **43**, 181 (2018).
- [2] P. G. Klemens, “The scattering of low-frequency lattice waves by static imperfections,” *Proc. Phys. Soc. A* **68**, 1113 (1955).
- [3] Joseph Callaway, “Model for Lattice Thermal Conductivity at Low Temperatures,” *Phys. Rev.* **113**, 1046–1051 (1959).
- [4] P. G. Klemens, “Thermal resistance due to point defects at high temperatures,” *Phys. Rev.* **119**, 507 (1960).
- [5] Miles V. Klein, “Phonon scattering by lattice defects,” *Phys. Rev.* **131**, 1500 (1963).
- [6] Ramya Gurunathan, Riley Hanus, Maxwell Dylla, Ankita Katre, and G. Jeffrey Snyder, “Analytical Models of Phonon-Point-Defect Scattering,” *Phys. Rev. Applied* **13**, 034011 (2020), arXiv:1910.03654.
- [7] Han Wei, Yue Hu, and Hua Bao, “Influence of point defects and multiscale pores on the different phonon transport regimes,” *Communications Materials* **4**, 3 (2023).
- [8] John M Ziman, *Electrons and phonons: the theory of transport phenomena in solids* (Clarendon Press, Oxford, 1960).
- [9] Natalio Mingo, K. Esfarjani, D. A. Broido, and D. A. Stewart, “Cluster scattering effects on phonon conduction in graphene,” *Phys. Rev. B* **81**, 045408 (2010).
- [10] Eleftherios N Economou, *Green’s functions in quantum physics*, 3rd ed. (Springer, Berlin, 1983).
- [11] A. Kundu, N. Mingo, D. A. Broido, and D. A. Stewart, “Role of light and heavy embedded nanoparticles on the thermal conductivity of SiGe alloys,” *Phys. Rev. B* **84**, 125426 (2011), arXiv:1108.6137.
- [12] Nakib Haider Protik, Jesús Carrete, Nebil A. Katcho, Natalio Mingo, and David Broido, “Ab initio study of the effect of vacancies on the thermal conductivity of boron arsenide,” *Phys. Rev. B* **94**, 045207 (2016).
- [13] Ankita Katre, Jesús Carrete, Bonny Dongre, Georg K.H. Madsen, and Natalio Mingo, “Exceptionally Strong Phonon Scattering by B Substitution in Cubic SiC,” *Phys. Rev. Lett.* **119**, 075902 (2017).
- [14] Carlos A Polanco and Lucas Lindsay, “Ab initio phonon point defect scattering and thermal transport in graphene,” *Phys. Rev. B* **97**, 014303 (2018).
- [15] Jonghoon Lee, Vikas Varshney, Ajit K. Roy, and Barry L. Farmer, “Single mode phonon energy transmission in functionalized carbon nanotubes,” *J. Chem. Phys.* **135**, 104109 (2011).
- [16] Hossein Honarvar, Lina Yang, and Mahmoud I. Hussein, “Thermal transport size effects in silicon membranes featuring nanopillars as local resonators,” *Appl. Phys. Lett.* **108**, 263101 (2016), arXiv:1605.02932.
- [17] R. Anufriev, R. Yanagisawa, and M. Nomura, “Aluminium nanopillars reduce thermal conductivity of silicon nanobeams,” *Nanoscale* **9**, 15083 (2017).
- [18] Hossein Honarvar and Mahmoud I. Hussein, “Two orders of magnitude reduction in silicon membrane thermal conductivity by resonance hybridizations,” *Phys. Rev. B* **97**, 195413 (2018), arXiv:1606.08591.
- [19] Joseph P. Feser, “Engineering heat transport in nanoparticle-in-alloy composites: The role of Mie scattering,” *J. Appl. Phys.* **125**, 145103 (2019).
- [20] Ongira Chowdhury and Joseph P. Feser, “Phonon scattering and vibrational localization in 2D embedded nanoparticle composites,” *J. Appl. Phys.* **131**, 194301 (2022).
- [21] Neil Zuckerman and Jennifer R Lukes, “Acoustic phonon scattering from particles embedded in an anisotropic medium: A molecular dynamics study,” *Phys. Rev. B* **77**, 094302 (2008).
- [22] Zhun-Yong Ong and Gang Zhang, “Efficient approach for modeling phonon transmission probability in nanoscale interfacial thermal transport,” *Phys. Rev. B* **91**, 174302 (2015).
- [23] Zhun-Yong Ong, “Tutorial: Concepts and numerical techniques for modeling individual phonon transmission at interfaces,” *J. Appl. Phys.* **124**, 151101 (2018).
- [24] Zhun-Yong Ong, “Atomistic  $S$ -matrix method for numerical simulation of phonon reflection, transmission, and boundary scattering,” *Phys. Rev. B* **98**, 195301 (2018).
- [25] N Mingo and Liu Yang, “Phonon transport in nanowires coated with an amorphous material: An atomistic Green’s function approach,” *Phys. Rev. B* **68**, 245406 (2003).
- [26] Jian-Sheng Wang, Jian Wang, and Nan Zeng, “Nonequilibrium Green’s function approach to mesoscopic thermal transport,” *Phys. Rev. B* **74**, 033408 (2006).
- [27] W Zhang, T S Fisher, and N Mingo, “Simulation of Interfacial Phonon Transport in Si-Ge Heterostructures Using an Atomistic Green’s Function Method,” *J. Heat Transfer* **129**, 483 (2007).
- [28] W Zhang, T S Fisher, and N Mingo, “The atomistic Green’s function method: an efficient simulation approach for nanoscale phonon transport,” *Numer. Heat Transfer, Part B* **51**, 333–349 (2007).
- [29] J-S Wang, Jian Wang, and J T Lü, “Quantum thermal transport in nanostructures,” *Eur. Phys. J. B* **62**, 381–404 (2008).
- [30] Hossein Khodavirdi, Zhun-Yong Ong, and Ankit Srivastava, “The Atomistic Green’s Function method for acoustic and elastic wave-scattering problems,” *Int. J. Mech. Sci.* **275**, 109263 (2024).
- [31] Zhun-Yong Ong, Georg Schusteritsch, and Chris J. Pickard, “Structure-specific mode-resolved phonon coherence and specularly at graphene grain boundaries,” *Phys. Rev. B* **101**, 195410 (2020), arXiv:2004.07424.
- [32] Zhun-Yong Ong, “Effect of boundary roughness on the attenuation of specular phonon reflection in graphene,” *Phys. Rev. B* **109**, 184207 (2024).
- [33] Ping Sheng, *Introduction to Wave Scattering, Localization and Mesoscopy*, 2nd ed. (Springer Berlin, Heidelberg, Heidelberg, Germany, 2006).
- [34] Ivana Savić, Natalio Mingo, and Derek A Stewart, “Phonon Transport in Isotope-Disordered Carbon and Boron-Nitride Nanotubes: Is Localization Observable?” *Phys. Rev. Lett.* **101**, 165502 (2008).
- [35] Abhishek Chaudhuri, Anupam Kundu, Dibyendu Roy, Abhishek Dhar, Joel L Lebowitz, and Herbert Spohn, “Heat transport and phonon localization in mass-disordered harmonic crystals,” *Phys. Rev. B* **81**, 064301 (2010).

- [36] Roger G Newton, *Scattering Theory of Waves and Particles*, 2nd ed. (Springer-Verlag Berlin Heidelberg, Berlin, 1982).
- [37] Luis J. Boya and Robert Murray, “Optical theorem in  $N$  dimensions,” *Phys. Rev. A* **50**, 4397 (1994).
- [38] Luis J. Boya, “Quantum-mechanical scattering in one dimension,” *Rivista del Nuovo Cimento* **31**, 75–139 (2008).
- [39] By flux-normalized, we mean that the absolute square of the wave eigenfunction gives us the flux, i.e.,  $j = |\Psi|^2 = 1$ .
- [40] A careful distinction should be made between the terms incident and incoming. The former is used to refer to the unperturbed state when the scatterer is absent while the latter is used to refer to the phonon mode that is traveling towards the device region. A rightward-propagating incident phonon consists of an incoming phonon eigenmode in the left lead and an outgoing phonon eigenmode in the right lead.
- [41] The Heaviside term  $\Theta(-v_{k'})$  eliminates the contributions from the transmitted rightward-propagating waves in Eq. (2).
- [42] J J Sakurai and Jim Napolitano, *Modern Quantum Mechanics*, 3rd ed. (Cambridge University Press, Cambridge, 2020).
- [43] Philip B Allen and Nhat A Nghiem, “Heat pulse propagation and nonlocal phonon heat transport in one-dimensional harmonic chains,” *Phys. Rev. B* **105**, 174302 (2022).
- [44] We specifically refer to the expression given by Eq. (A.3) in Ref. [43].
- [45] L Lindsay and D A Broido, “Optimized Tersoff and Brenner empirical potential parameters for lattice dynamics and phonon thermal transport in carbon nanotubes and graphene,” *Phys. Rev. B* **81**, 205441 (2010).
- [46] Masato Ohnishi and Junichiro Shiomi, “Strain-induced band modulation of thermal phonons in carbon nanotubes,” *Phys. Rev. B* **104**, 014306 (2021).
- [47] Julian D Gale and Andrew L Rohl, “The general utility lattice program (GULP),” *Mol. Simul.* **29**, 291–341 (2003).
- [48] M S Dresselhaus and P C Eklund, “Phonons in carbon nanotubes,” *Advances in Physics* **49**, 705–814 (2000).
- [49] G. D. Mahan, “Oscillations of a thin hollow cylinder: Carbon nanotubes,” *Phys. Rev. B* **65**, 235402 (2002).
- [50] L. Chico, R. Pérez-Álvarez, and C. Cabrillo, “Low-frequency phonons in carbon nanotubes: A continuum approach,” *Phys. Rev. B* **73**, 075425 (2006).
- [51] Jian Sheng Wang, Bijay Kumar Agarwalla, Huanan Li, and Juzar Thingna, “Nonequilibrium Green’s function method for quantum thermal transport,” *Front. Phys.* **9**, 673–697 (2014), arXiv:1303.7317.
- [52] Daniel S Fisher and Patrick A Lee, “Relation between conductivity and transmission matrix,” *Phys. Rev. B* **23**, 6851–6854 (1981).
- [53] P A Khomyakov, G Brocks, V Karpan, M Zwierzycki, and P J Kelly, “Conductance calculations for quantum wires and interfaces: Mode matching and Green’s functions,” *Phys. Rev. B* **72**, 035450 (2005).
- [54] Natalio Mingo, “Green’s Function Methods for Phonon Transport Through Nano-Contacts,” in *Thermal Nanosystems and Nanomaterials* (Springer, Heidelberg, 2009) pp. 63–94.
- [55] T Ando, “Quantum point contacts in magnetic fields,” *Phys. Rev. B* **44**, 8017–8027 (1991).
- [56] Dhruv Singh, Jayathi Y Murthy, and Timothy S Fisher, “Effect of phonon dispersion on thermal conduction across Si/Ge interfaces,” *J. Heat Transfer* **133**, 122401 (2011).
- [57] Sridhar Sadasivam, Yuhang Che, Zhen Huang, Liang Chen, Satish Kumar, and Timothy S Fisher, “The atomistic Green’s function method for interfacial phonon transport,” *Ann. Rev. Heat Transfer* **17**, 89–145 (2014).
- [58] Qichen Song and Gang Chen, “Evaluation of the diffuse mismatch model for phonon scattering at disordered interfaces,” *Phys. Rev. B* **104**, 085310 (2021), arXiv:2106.04745.